Finite Element Based Multi-Objective Optimization of a Brushless Doubly-Fed Induction Machine

Tim D. Strous, Xuezhou Wang, Henk Polinder, *Senior Member, IEEE*, J. A. (Bram) Ferreira, *Fellow, IEEE*

***Abstract*—Although the brushless DFIM has great potential as generator system in large-scale wind turbines, its complexity has so far retained a commercial breakthrough. This paper contributes by combining brushless DFIM FE modelling with multi-objective optimization. A static brushless DFIM FE model is applied with the NSGA-II multi-objective optimization algorithm. The result is an accurate and fast brushless DFIM design optimization tool. This tool is then used to generate a machine design with optimized performance, that fits a fixed volume frame size D180. Optimization results of different brushless DFIM construction variations are compared. The best designs of each construction variation are then analysed in more detail using a time-stepping brushless DFIM FE model. This provides good insight in the effects of different construction variations on torque ripple and induced time-harmonics. The optimized design of the best construction variation will be selected to be manufactured as prototype machine.**

***Index Terms*—Brushless Doubly-Fed Machine (BDFM), Cross coupling, DFIG, FE modeling, Harmonics, Multi Objective Optimization, Nested-loop Rotor, Torque Ripple.**

I. Introduction

WIND technology has majored over the last decades. This has led to a substantial amount of installed wind capacity from commercially developed wind turbines worldwide. The current trend of taking wind turbines off-shore increases the need for more reliable and fault-tolerant wind turbine generator designs [1]. That is why the brushless Doubly-Fed Induction Machine (DFIM) has gained an increasing research interest in recent years. This machine type has the same operating characteristics as the normal DFIG, commonly applied in wind turbines. However, this machine provides several additional advantages, which include [2]:

- No brush gear and slip rings; increasing robustness and reliability, while decreasing the need for maintenance.
- A low-speed machine-type; enables the reduction of the number of gear stages, which increases reliability.
- Improved capabilities to comply with current grid-code requirements [3].

Despite its potential as generator system for large scale wind turbines the brushless DFIM has never been commercially exploited.

The brushless DFIM consists of two stator windings with different pole-pair numbers, one stator winding, the Power-Winding (PW), is connected to the grid while the other stator winding, the Control-Winding (CW), is connected to a partially rated PE converter. Because both windings have different pole-pair numbers, there is no magnetic coupling between them. However, a special nested-loop rotor structure ensures coupling to both windings. Hence the two stator windings are magnetically cross-coupled [4]. Figure 1 provides a schematic view of a brushless DFIM incorporated in a wind turbine drive-train.

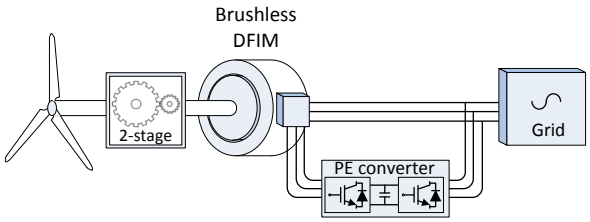

Fig. 1. Brushless DFIM incorporated in a wind turbine drive-train.

The complexity of the brushless DFIM machine type results in the need for more sophisticated models, since effects such as time- and space-harmonic components as well as saturation are far more dominant in this machine type [2], [5]. Techniques such as Electric Equivalent Circuit (EEC) modelling have proven to be useful in presenting and explaining the brushless DFIM operating characteristics [6], but deriving accurate circuit parameters is challenging [7]. Recently other analytical modelling techniques have been developed, such as Magnetic Equivalent Circuit (MEC) modelling, providing reasonable accuracy and better results compared to EC models [8]. In [2] an accurate magnetic field model is presented, however the effects of saturation are neglected. More accurate models have been developed with the use of Finite Element (FE) methods [9], [10]. However, these models are far more time-consuming. Recently [11] developed a magneto-static brushless DFIM FE model which was an order of 100 times less time-consuming as conventional time-stepping FE methods. The model is limited to calculate steady-state operating points only, but it is suitable for implementation in optimization algorithms.

Optimization is an important topic for machine design. The accuracy of the optimization results depend in large on the accuracy and speed of the applied machine models. Literature shows attempts of combining brushless DFIM models with optimization routines to improve already existing machine designs. In [12], brushless DFIM EEC modeling in combination with thermal modeling is applied in a multi-objective optimization

The research leading to these results has received funding from the European Union's Seventh Framework Programme managed by REA Research Executive Agency (FP7/2007_2013) under Grant Agreement N.315485.

T. D. Strous, X. Wang, H. Polinder and J. A. Ferreira are with the Department of Electrical Sustainable Energy, Delft University of Technology, The Netherlands (e-mail: t.d.strous@tudelft.nl)

algorithm to improve the power to weight ratio of a brushless DFIM design. However, this approach lags the accuracy of FE modeling.

This paper contributes by combining brushless DFIM FE modelling with multi-objective optimization in order to create a fast, accurate and flexible brushless DFIM design optimization tool. The proposed design method uses the fast solving magneto-static brushless DFIM FE model from [11] in combination with the NSGA-II multi-objective optimization algorithm [13]. This design method is then used to generate a machine design with optimized performance, that fits a fixed volume frame size D180. Optimization results of different brushless DFIM construction variations are compared. The best designs of each construction variation are selected and are analysed in more detail using a conventional time-stepping brushless DFIM FE model. This provides additional insight in the effects of different construction variations on torque ripple and induced time-harmonics. One optimized design will be selected to be manufactured as prototype machine for further studies.

II. Brushless DFIM Design Optimization

A. Optimization Procedure

For optimization of electrical machines there are many variables to consider. Those can include construction variations, as well as geometric variables. Additionally, several optimization objectives can be determined. The brushless DFIM optimization procedure is schematically presented in figure 2. Based on the input parameters, containing machine construction parameters, geometric parameters and material properties, the complete machine geometry is calculated using a geometric model developed in Matlab. This ensures that the complete machine geometry is parameter based and therefore more suitable for optimization. Using a Matlab-Comsol interface, the machine geometry is then loaded to the magneto-static brushless DFIM FE model developed in Comsol [11]. The FE model analyses the machines nominal performance. For optimization the NSGA-II (non-dominated sorting genetic algorithm II) is applied [13]. This well-known evolutionary based algorithm is able to determine Pareto optimal solutions to multi-objective problems. A first population of N machine designs is generated and evaluated by the magneto-static brushless DFIM FE model. Each individual design varies based on a set of provided geometric input variables V. All N machine designs are evaluated according the optimization objectives and a new generation of N machine designs is generated from the best (fittest) individuals of the previous generation.

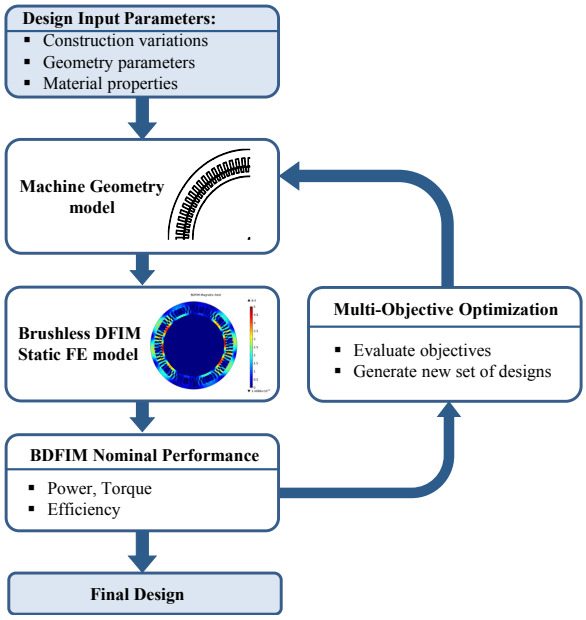

Fig. 2. Brushless DFIM design optimization procedure.

B. Optimization of a Brushless DFIM Prototype Design

The study in this paper focusses on the performance optimization of a prototype brushless DFIM design that fits a fixed frame size D180. Since the volume of this machine is fixed the brushless DFIM design will be optimized for both power/torque and efficiency. Table I provides an overview of fixed design parameters. Since the brushless DFIM is a synchronous machine type, it's nominal operating point depends on the rotor position relative to the stator magnetic field. For the provided PW and CW current density levels, maximum torque is generated at a rotor position shift γ_{shift} of $1/4^{th}$ of a rotor nest span, this point is selected as the machines nominal operating point.

The optimization is performed for different brushless DFIM construction variations. These construction variations are presented in table II. Here p_p and p_c are the number of pole-pairs for respectively the power- and control-winding. N_{ss} is the number of stator slots, which affects the number of slots per pole per phase of both power- and control-winding. q_r is the number of loops per rotor nest. The optimization algorithm parameters and optimization variables, are presented in table III. Since the machine volume is already fixed the number of geometric optimization variables V will be limited.

TABLE I
Brushless DFIM Design Parameters

Construction Parameters		
PW Number of phases	N_{ph}	3
CW Number of phases	N_{ph}	3
Geometric Parameters		
Axial stack length	l_{stk}	0.24 m
Air-gap length	l_g	1.0 mm
Stator outer radius	r_{so}	0.135 m
Rotor inner radius	r_{ri}	0.035 m
PW/CW Stator slot area ratio		50% / 50%
Stator/rotor tooth tip height		$1/16^{th}$ tooth height
Stator/rotor tooth tip width		50% closed
Nominal operating point		
PW frequency	f_{pe}	50 Hz
PW slot current density	$J_{p,slot}$	1 A/mm^2
CW frequency	f_{ce}	-10 Hz
CW slot current density	$J_{c,slot}$	1 A/mm^2
Initial rotor position	γ_{shift}	$(90/N_{nest})^\circ$

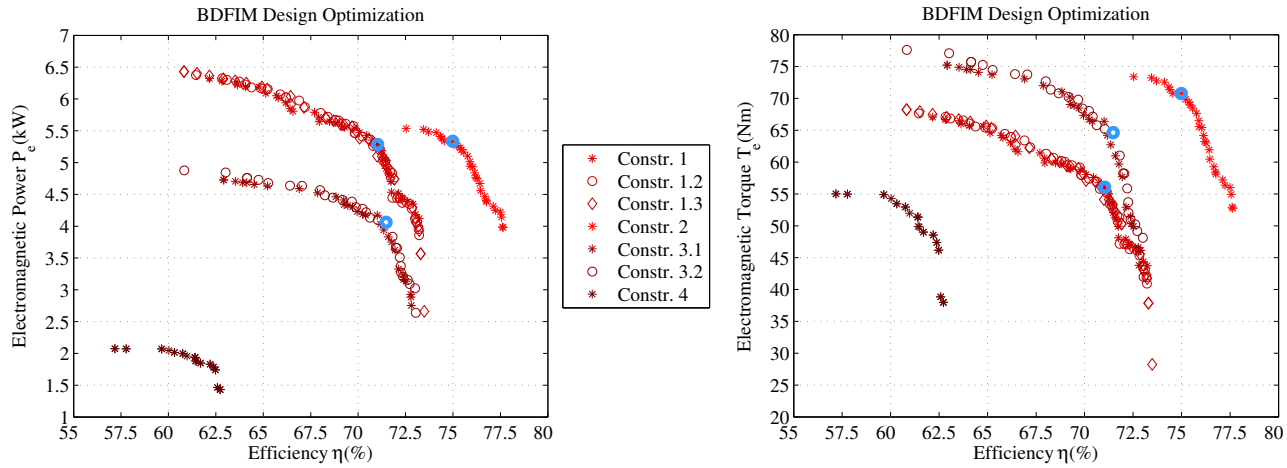

(a) Efficiency vs. electromagnetic power

(b) Efficiency vs. electromagnetic torque

Fig. 3. BDFIM design optimization results for different construction variations

For this study both output power and efficiency are selected as optimization objectives. There will be a trade-off between electromagnetic output power and efficiency, more efficient machine designs will result in less electromagnetic output power.

TABLE II
BRUSHLESS DFIM CONSTRUCTION VARIATIONS

	p_p	p_c	N_{ss}	q_r
Construction 1.1	1	3	54	4
Construction 1.2	1	3	54	5
Construction 1.3	1	3	72	5
Construction 2	2	3	72	5
Construction 3.1	2	4	72	4
Construction 3.2	2	4	72	5
Construction 4	4	6	72	3

TABLE III
BRUSHLESS DFIM DESIGN OPTIMIZATION

Optimization Settings		
Method		NSGA-II
Objectives		2
Variables	V	5
Constraints		0
Population size	N	30
Generations		40
Calculation time single generation		38 $min.$
FE elements per design		$\pm$ 20e3 quadratic

Geometric Optimization Variables		**min**	**max**
Stator inner radius	r_si	0.05 m	0.11 m
Ratio stator slot/yoke height	$\alpha_{s,y}$	0.2	0.8
Ratio rotor slot/yoke height	$\alpha_{r,y}$	0.2	0.8
Ratio stator inner/max slot width	$\alpha_{s,sw}$	0.2	0.8
Ratio rotor inner/max slot width	$\alpha_{r,sw}$	0.2	0.8

The optimization results are presented in figure 3. The optimization for each construction variation as presented in table II, leads to a Pareto front of optimization results, along the efficiency η and electromagnetic output power P_e or Torque T_e axes.

From figure 3a can be observed that brushless DFIM constructions with higher pole-pair numbers result in machine designs that generate lower power at lower efficiency. This is obvious, since machines with higher pole-pair combinations rotate at lower mechanical speed. Therefore it is better to compare machine variations based on generated torque, as is done in figure 3b. Furthermore can be observed that a varying number of loops per nest q_r and number of stator slots N_{ss} seem to have little influence on the nominal performance. However, it can be expected that these parameters will affect the level of torque ripple and harmonic pollution of a machine design. From figure 3 can further be concluded that a brushless DFIM design with pole-pair combination $p_p = 2$ and $p_c = 3$ yields the best performance in terms of efficiency and generated torque. However, a brushless DFIM with this pole-pair combination is subject to unbalanced magnetic pull [14]. For small prototype machines such as a D180 frame size, unbalanced magnetic pull is expected to be less harmful to the machine. Therefore the machine construction variation with $p_p = 2$ and $p_c = 3$ seems to be the favourable construction variation for the prototype machine design.For this construction variation, the construction variations with pole-pair combination $p_p = 1$ and $p_c = 3$ and the construction variations with pole-pair combination $p_p = 2$ and $p_c = 4$, a most suitable machine design candidate. Resulting in three machine design candidates selected from the optimization results (blue dots in figure 3). These three optimized machine design candidates of different pole-pair combination will additionally be analysed with a time-stepping brushless DFIM FE model. This will be discussed in the next section.

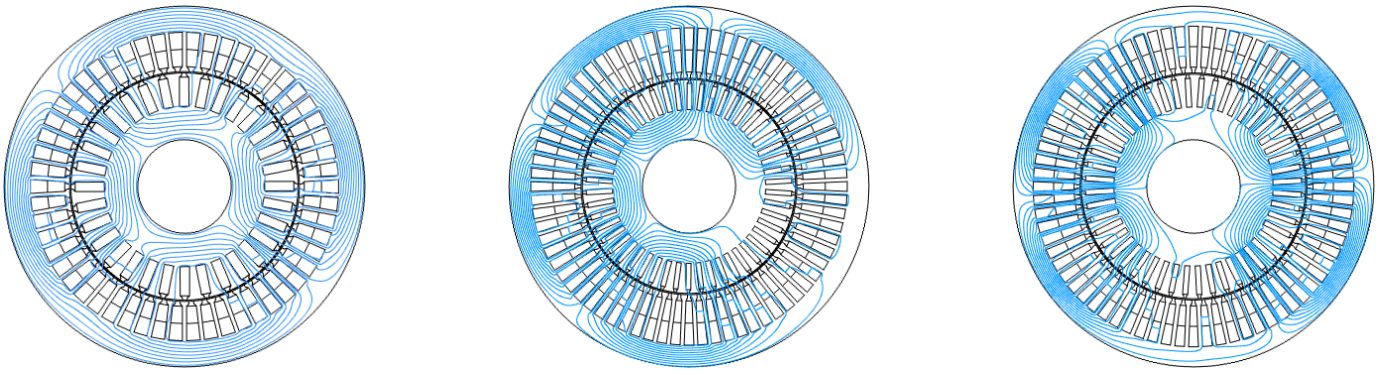

(a) $p_p = 1, p_c = 3, N_{ss} = 54, q_r = 4$ (b) $p_p = 2, p_c = 3, N_{ss} = 72, q_r = 5$ (c) $p_p = 2, p_c = 4, N_{ss} = 72, q_r = 4$

Fig. 4. Optimized machine design geometries for different construction variations (including magnetic field lines)

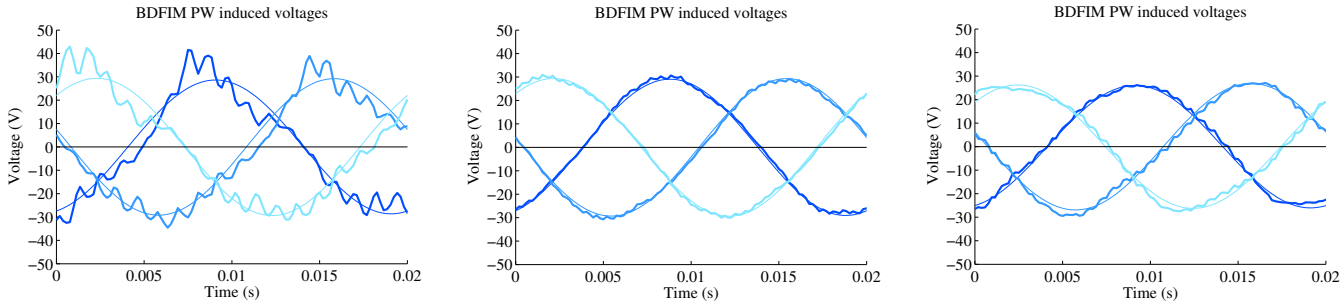

(a) $p_p = 1, p_c = 3, N_{ss} = 54, q_r = 4$ (b) $p_p = 2, p_c = 3, N_{ss} = 72, q_r = 5$ (c) $p_p = 2, p_c = 4, N_{ss} = 72, q_r = 4$

Fig. 5. Single-turn induced phase voltages in the PW, including main harmonic components

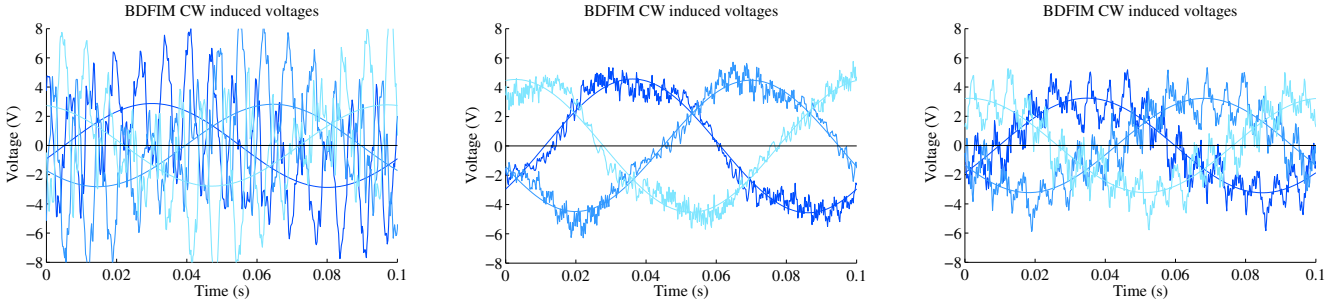

(a) $p_p = 1, p_c = 3, N_{ss} = 54, q_r = 4$ (b) $p_p = 2, p_c = 3, N_{ss} = 72, q_r = 5$ (c) $p_p = 2, p_c = 4, N_{ss} = 72, q_r = 4$

Fig. 6. Single-turn induced phase voltages in the CW, including main harmonic components

III. Comparison of Brushless DFIM Construction Variations

From the optimization results three machine designs with different construction variation were selected for further evaluation. Because of the natural rich space-harmonic spectrum of the brushless DFIM, effects as torque ripple and time-harmonic distortion can be more severe. These effects depend mostly on the selected construction variation [9]. Using a time-stepping brushless DFIM FE model, the selected machine designs are modelled and simulated in their nominal operating point for 2 rotor electric periods f_{re}. The resulting power- and control-winding voltages, rotor currents and torque responses are presented in figures 5 till 8. Figure 4 presents the 2D geometries of the three selected machine design candidates, including their magnetic field lines at time = 0.

Using (1) the torque ripple can be determined from the simulation results (Figure 8). The mean torque T_{mean} and torque ripple T_{ripple} comparison results are presented in table IV.

$$T_{ripple} = \frac{T_{e,\max} - T_{e,\min}}{T_{e,mean}} \cdot 100\% \qquad (1)$$

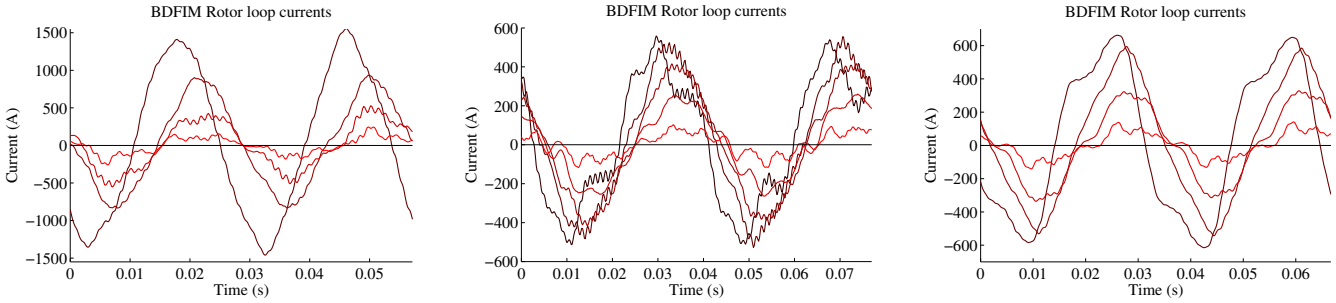

(a) $p_p = 1, p_c = 3, N_{ss} = 54, q_r = 4$ (b) $p_p = 2, p_c = 3, N_{ss} = 72, q_r = 5$ (c) $p_p = 2, p_c = 4, N_{ss} = 72, q_r = 4$

Fig. 7. Induced rotor loop currents

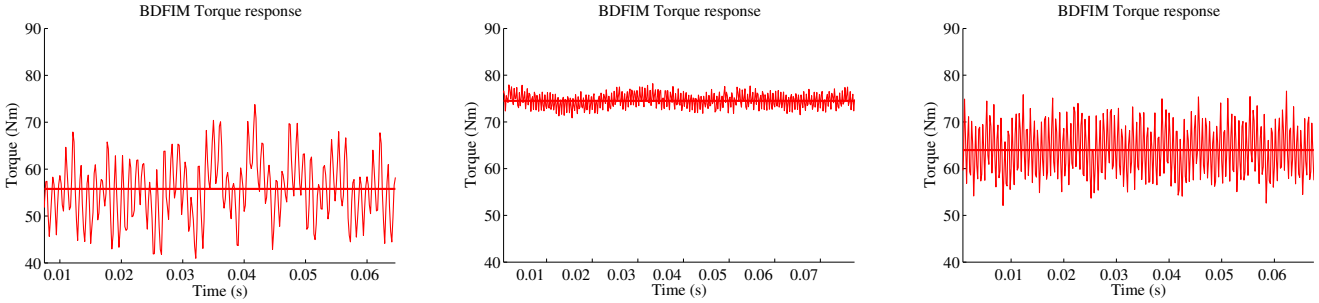

(a) $p_p = 1, p_c = 3, N_{ss} = 54, q_r = 4$ (b) $p_p = 2, p_c = 3, N_{ss} = 72, q_r = 5$ (c) $p_p = 2, p_c = 4, N_{ss} = 72, q_r = 4$

Fig. 8. Torque response, including main torque

The severity of induced time-harmonic components in the induced power-winding voltage e_{PW}, control-winding voltage e_{CW} and in the currents of the rotor nested loops is compared by calculating the Total Harmonic Distortion (THD_F):

$$THD_F = \frac{\sqrt{\sum_{h=2}^{\infty} V_{(h)}^2}}{V_{(1)}} \cdot 100\% \qquad (2)$$

The comparison results of the THD_F of the power- and control-winding voltage and the currents in the different rotor nested loops are presented in Table V.

From the comparison results in Table IV and V it can be observed that all brushless DFIM design variations suffer from an excessive space-harmonic spectrum. While the results show clearly that the selection of a suitable combination of pole-pairs for a brushless DFIM design can reduce the detrimental effects of a rich space-harmonic spectrum, additional measures should be taken to reduce the torque ripple and induced time-harmonics even more. This could be achieved by applying skew

TABLE IV
BRUSHLESS DFIM TORQUE RIPPLE COMPARISON

Construction Variation:	$T_{mean}(Nm)$:	$T_{ripple}(\%)$:
1: $p_p = 1, p_c = 3$	55.6	59.0
2: $p_p = 2, p_c = 3$	74.6	9.8
3: $p_p = 2, p_c = 4$	64.0	38.3

TABLE V
BRUSHLESS DFIM HARMONIC DISTORTION COMPARISON

	$THD_F(\%)$:		$THD_F(\%)$:				
Construction:	e_{PW}	e_{CW}	I_{r1}	I_{r2}	I_{r3}	I_{r4}	I_{r5}
1: $p_p = 1, p_c = 3$	23.5	154.1	5.7	9.3	20.8	43.1	
2: $p_p = 2, p_c = 3$	4.5	14.2	24.3	9.9	7.0	15.0	43.8
3: $p_p = 2, p_c = 4$	7.9	45.2	21.1	10.8	14.3	33.8	

to the rotor, as is also done in most other electrical machines. It is worthwhile to remark that the harmonic distortion of the control-winding voltages also depends on the control-winding frequency f_{ce}. The main component of the control-winding voltage e_{CW} is proportional to it's frequency, however the induced time-harmonic components are not. Therefore, if the control winding frequency approaches zero the control-wining voltage THD_F will goes to infinity.

From the comparison results it can be concluded that the brushless DFIM of construction variation 2 (with $p_p = 2$ and $p_c = 3$), produces the highest electromagnetic torque and the lowest torque ripple. Also the harmonic distortion of the voltage signals is lowest. Resulting in less grid pollution and a more stable control. Therefore a brushless DFIM of construction variation 2 can be considered the most favourable for small machine types such as a frame-size D180 prototype machine. Further, from table V can be observed that the loop span of the loops in a nested-loop rotor influences the level of

harmonic distortion. This could be used in future research for optimization of the loop-span of rotor inner loops.

IV. Conclusion

This paper combined multi-objective optimization with a magneto-static brushless DFIM FE model. The result is a fast, flexible and accurate machine optimization approach that can be used for brushless DFIM design purposes. This novel design approach was then used for the design of a fixed frame-size D180 brushless DFIM prototype machine. This machine design was optimized for both maximum generated electromagnetic power/torque and efficiency. The optimization was performed for several brushless DFIM construction variations with different pole-pair combinations, different numbers of loops per rotor nest and different number of stator slots. Within these construction variations, only the chosen pole-pair combination seems to have a significant influence on the obtainable electromagnetic torque and efficiency output performance. For each considered brushless DFIM construction, with a different pole-pair combination, the best design candidate was selected from the optimization results for further analysis with a time-stepping brushless DFIM FE model. Three different machine construction variations were evaluated in this manner to determine the effects of torque ripple and time-harmonic distortions of the voltage and currents. It can be concluded that the chosen pole-pair combination also has a large influence on torque ripple and induced time-harmonics. A brushless DFIM construction with a pole-pair combination of $p_p = 2$ and $p_c = 3$ seems to be favourable over other construction variations with different pole-pair combinations. This construction variation generates the highest output performance as well as the least torque ripple and induced time-harmonics. Therefore, the optimized design of this brushless DFIM construction variation is selected to be manufactured as prototype machine for future studies.

References

[1] R. A. McMahon, X. Wan, E. Abdi-Jalebi, P. Tavner, P. C. Roberts, and M. Jagiela, "The bdfm as a generator in wind turbines," in *12th Int. Power Electron. and Motion Control Conf., EPE-PEMC.*, 2006, pp. 1859–1865.

[2] T. D. Strous, N. H. van der Blij, H. Polinder, and J. A. Ferreira, "Brushless doubly-fed induction machines: Magnetic field modelling," in *Int. Conf. Elect. Machines (ICEM)*, Sep. 2014, pp. 2702–2708.

[3] U. Shipurkar, T. D. Strous, H. Polinder, and J. A. Ferreira, "Lvrt performance of brushless doubly-fed induction machines - a comparison," in *Int. Conf. Elect. Machines & Drives (IEMDC), 2015*, to be presented at.

[4] E. Wiedenbrug, M. Boger, A. Wallace, and D. Patterson, "Electromagnetic mechanism of synchronous operation of the brushless doubly-fed machine," in *Conf. Rec. Ind. Applicat. IEEE 13th IAS Annual Meeting*, vol. 1, 1995, pp. 774–780.

[5] H. Gorginpour, B. Jandaghi, and H. Oraee, "Time and space harmonics in brushless doubly-fed machine," in *19th Iranian Conf. Elect. Eng. (ICEE)*, 2011, pp. 1–6.

[6] T. Logan and R. McMahon, "Operating charts for the brushless doubly-fed machine (bdfm)," in *IEEE Int. Elect. Machines and Drives Conf. (IEMDC)*, 2009, pp. 1276–1283.

[7] P. Roberts, R. McMahon, P. Tavner, J. Maciejowski, and T. Flack, "Equivalent circuit for the brushless doubly fed machine (bdfm) including parameter estimation and experimental verification," *IEE Proc. -Electric Power Applicat.*, vol. 152, no. 4, pp. 933–942, 2005.

[8] H. Gorginpour, H. Oraee, and R. McMahon, "A novel modeling approach for design studies of brushless doubly fed induction generator based on magnetic equivalent circuit," *IEEE Trans. Energy Convers.*, vol. 28, no. 4, pp. 902–912, 2013.

[9] N. van der Blij, T. Strous, X. Wang, and H. Polinder, "A novel analytical approach and finite element modelling of a bdfim," in *Int. Conf. Elect. Machines (ICEM)*, 2014, pp. 346–352.

[10] A. Ferreira and S. Williamson, "Time-stepping finite-element analysis of brushless doubly fed machine taking iron loss and saturation into account," *IEEE Trans. Ind. Appl.*, vol. 35, no. 3, pp. 583–588, 1999.

[11] X. Wang, T. D. Strous, D. Lahaye, H. Polinder, and J. A. Ferreira, "Finite element modeling of brushless doubly-fed induction machine (bdfim) based on magneto-static simulation," in *Int. Conf. Elect. Machines & Drives (IEMDC), 2015*, to be presented at.

[12] H. Gorginpour, H. Oraee, and R. McMahon, "Electromagnetic-thermal design optimization of the brushless doubly fed induction generator," *IEEE Trans. Ind. Electron.*, vol. 61, no. 4, pp. 1710–1721, 2014.

[13] K. Deb, A. Pratap, S. Agarwal, and T. Meyarivan, "A fast and elitist multiobjective genetic algorithm: NSGA-II," *IEEE Trans. Evol. Comput.*, vol. 6, no. 2, pp. 182–197, 2002.

[14] S. Abdi, E. Abdi, and R. McMahon, "A study of unbalanced magnetic pull in brushless doubly fed machines," *IEEE Trans. Energy Convers.*, to be published, early Access.

V. Biographies

T. D. Strous received the M.Sc. degree in electrical engineering from Delft University of Technology, Delft, The Netherlands, in 2010. Currently he is working towards the Ph.D. degree in the field of electrical machines. His current research interests include modelling and design of electrical machines and drives.

Xuezhou Wang received the M.Sc. in power electronics and electrical drives from Northwestern Polytechnical University, Xian, China, in 2013. Currently he is working towards his PhD degree in the field of electrical machines. His current research interests include numerical modelling and design of electrical machines.

H. Polinder received the MSc and the PhD degree from Delft University of Technology, Delft, The Netherlands, in 1992 and 1998. Since 1996 he has been an assistant/associate professor in the Electrical Power Processing Group of Delft University of Technology. He worked part-time at Lagerwey in Barneveld in 1998/1999, at Philips Applied Technologies in Eindhoven in 2002 and at ABB Corporate Research in Vasteras in 2008. He was a visiting professor at the University of Newcastle-upon-Tyne in 2002, at Laval University, Quebec in 2004 and at the University of Edinburgh in 2006. He is author or coauthor of over 200 papers. His research interests include design aspects of electrical machines, mainly for renewable energy applications.

J. A. Ferreira received the B.Sc.Eng., M.Sc..Eng., and Ph.D. degrees in Electrical Engineering from the Rand Afrikaans University, Johannesburg, South Africa in 1981, 1983 and 1988 respectively. In 1981 he was with the Institute of Power Electronics and Electric Drives, Technical University of Aachen, and worked in industry at ESD (Pty) Ltd from 1982-1985. From 1986 until 1997 he was at the Faculty of Engineering, Rand Afrikaans University, where he held the Carl and Emily Fuchs Chair of Power Electronics in later years. Since 1998 he is a professor at the Delft University of Technology in The Netherlands. Dr. Ferreira is a fellow of the IEEE.